Review Article

Terahertz Spectroscopy of Novel Superconductors

Stefano Lupi

CNR-IOM and Department of Physics, Sapienza, University of Rome, P.le A. Moro 2, 00185 Rome, Italy

Correspondence should be addressed to Stefano Lupi, stefano.lupi@roma1.infn.it

Through the coupling of Synchrotron Radiation and Michelson interferometry, one may obtain in the terahertz (THz) range transmittance and reflectivity spectra with a signal-to-noise ratio (S/N) up to 10^3. In this paper we review the application of this spectroscopic technique to novel superconductors with an increasing degree of complexity: the single-gap boron-doped diamond; the isotropic multiband V_3Si, where superconductivity opens two gaps at the Fermi energy; the CaAlSi superconductor, isostructural to MgB_2, with a single gap in the hexagonal ab plane and two gaps along the orthogonal c axis.

1. Introduction

After the discovery of high-T_c cuprates in 1986 that renewed the interest on superconducting materials, many new superconductors with different transport and magnetic properties have been synthesized in recent years. Among them one may cite A-doped (A = K, Rb, Na) C_{60}, Na_xCoO_2 codoped with H_2O; MgB_2 and CaAlSi, and Boron-doped diamond and the new Iron pnictides. The magnetic, transport, and electrodynamics properties of a superconductor are intimately related to few parameters: the critical temperature T_c, the value and the symmetry in the k space of the superconducting gap $\Delta(k)$, the critical magnetic fields H_{C1}, and H_{C2}, and the penetration depth λ. The main issue about a new superconductor concerns if these properties can be described through the mean-field Bardeen-Cooper-Schrieffer (BCS) theory (which well-captures the properties of conventional superconducting metals), or a different, more exotic, theory should be considered. For instance, strongly covalent bonds, high-concentration of impurities, and high-phonon frequencies make B-doped diamond much different from the conventional metals where the BCS model holds. Moreover, after the discovery of MgB_2, multiple-band unconventional-coupling superconductivity has been put forward and the properties of known materials like V_3Si, with several electronic bands crossing the Fermi energy (E_F), and recently discovered CaAlSi with anisotropic lattice properties, have been investigated in this scenario.

The presence of a gap in the electronic excitations near the Fermi level for $T < T_c$, is one of the main effect induced by superconductivity [1]. If the Cooper pairs are in a spherically symmetric s-state this gap opens along all directions of the Brillouin zone. When more bands cross E_F, they can be characterized by different superconducting gaps if a low interband scattering is present. However, if a p or a d type band (or a linear combination) defines the electronic properties of the system, the gap (gaps) opens only along particular k directions. This is the case for high-T_c cuprates and, probably, for iron pnictides.

THz spectroscopy is a powerful experimental tool to characterize superconductor materials, as it probes directly, and with the highest spectral resolution, their low-energy bulk electrodynamics. The optical properties of a material can be described through the reflectivity R and/or the transmittance T. In an isotropic metallic superconductor and below T_c, R reaches the value 1 for any frequency $\omega < 2\Delta(T)$ where $\Delta(T)$ is the superconducting gap. In the normal state and in the same low-frequency range, $R(T)$ follows a metallic behavior characterized by a plasma frequency ω_p and a scattering rate $\Gamma(T)$. If the metal is in the "dirty" regime defined by $\Gamma(T_c) > 2\Delta(0)$, the ratio $R_S(T < T_c)/R_N$ between the reflectivity in the superconducting state R_S and that in the normal state R_N exhibits a peak [1] at $2\Delta(T)$ and the same happens for the ratio $T_S(T < T_c)/T_N$. Both the value of $2\Delta(T)$ and its temperature dependence can be easily compared with the BCS predictions. For example,
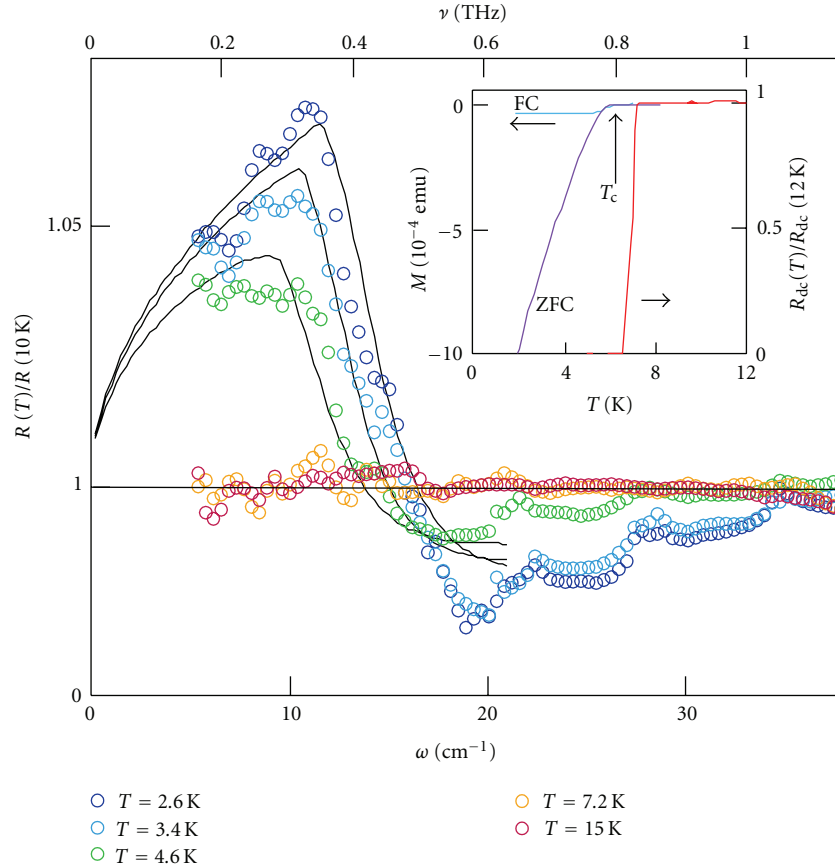
FIGURE 1: Reflectivity of a B-doped diamond film in the sub-THz region at different T normalized to its value at 10 K. The lines are fits obtained by assuming a BCS reflectivity below T_c and a Hagen-Rubens model at 10 K. The inset shows on the left scale the magnetic moment of the sample, as cooled either in a 10 Oe field (FC) or in zero field (ZFC), on the right scale its resistance normalized to its value at 12 K. The FC values are multiplied by 10.

in the weak coupling limit of the original BCS model $2\Delta(0) = 3.53T_c$, and for most of superconductors $2\Delta(0)$ ranges in the terahertz region (1 THz = 33 cm^{-1} = 4 meV = 333 μm).

In the experiments, however, one may encounter serious difficulties to measure the small difference between R_S (T_S) and R_N (T_N), as R_N in a good metal may be as high as 0.99 in the range of frequencies $\omega \sim 2\Delta$. Therefore, a signal-to-noise ratio on the order of 10^3 is often needed in the terahertz region to measure the superconducting gap. Nowadays, this strong requirement can be fulfilled with a conventional Michelson interferometric apparatus, when it is coupled to Infrared (IR) and THz Synchrotron Radiation (SR). SR sources with these characteristics are routinely open to users in Europe at the infrared beamlines SISSI [3] and IRIS [4] of the storage rings ELETTRA and BESSY-II, respectively.

In this paper we will review the IR and THz properties of three different superconductors with an increasing degree of complexity: the B-doped diamond, where we will show that a phononic BCS theory well-describes its superconducting properties; the V$_3$Si A15-type system, where two main electronic bands contribute to the density of states (DOS) near

E_F and its electrodynamics properties are associated with two superconducting gaps; finally CaAlSi, a superconductor, isostructural to MgB$_2$, with a single gap in the hexagonal ab plane and two gaps along the orthogonal c axis.

2. The Optical Gap of Superconducting Diamond

The sample here investigated was a $3\,\mu$m thick film 2.5×2.5 mm wide, grown by Chemical Vapor Deposition technique (CVD) and deposited on a pure CVD diamond substrate [5]. This thickness, assuring a zero transmittance in the THz range, provides us to probe the bulk response of the B-doped material.

X-ray diffraction patterns collected just after the growth showed that the whole film surface had an (111) orientation, with no appreciable spurious contributions, as already reported for similar samples [6]. The boron concentration was estimated to be nearly 6×10^{21} cm^{-3}, that is over the metal-to-insulator transition limit. The sample magnetic moment $M(T)$, reported in the inset of Figure 1 shows a superconducting transition with an onset at $T_c = 6$ K.
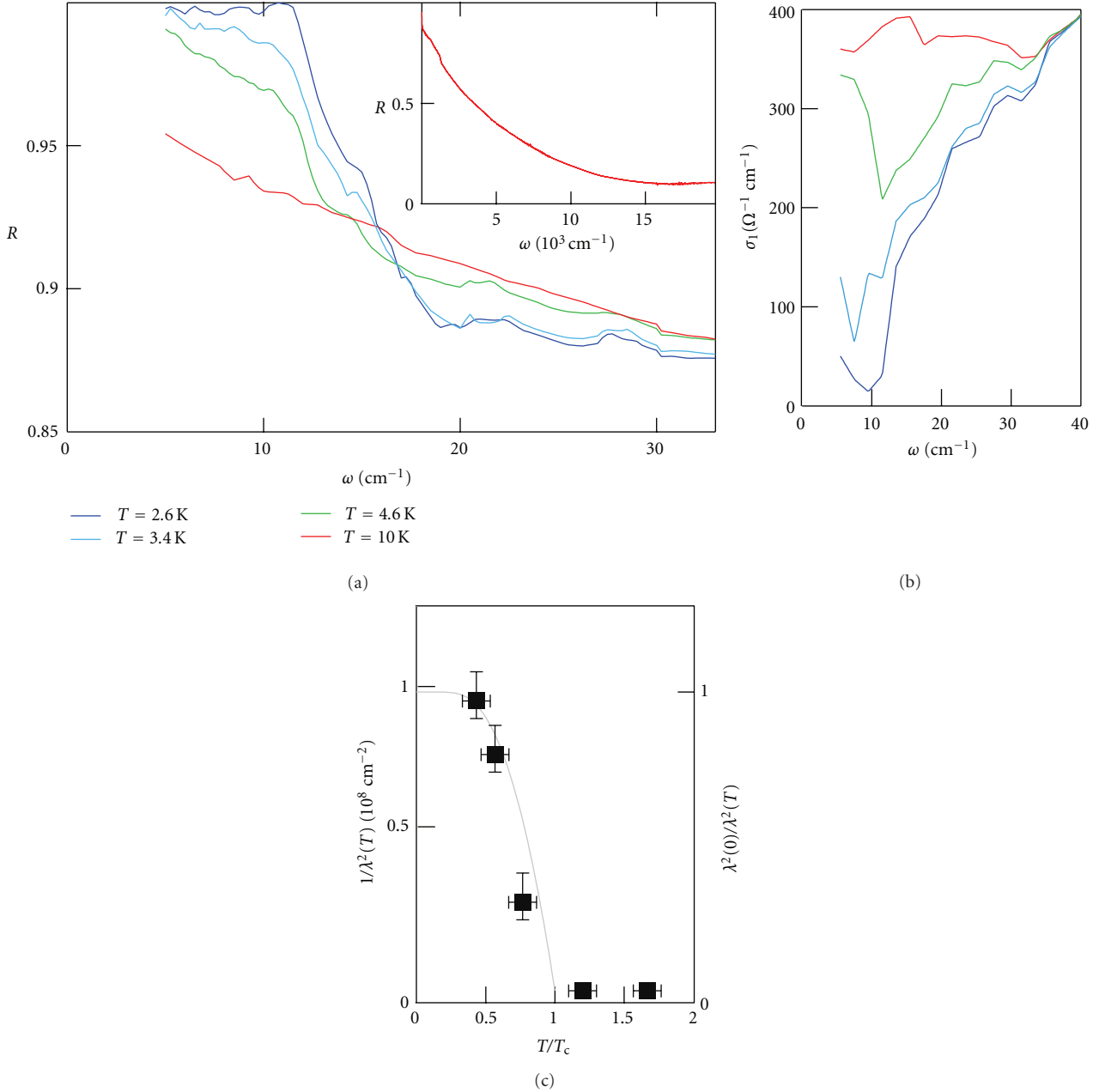
(a)

(b)

(c)

FIGURE 2: Infrared behavior of superconducting diamond. (a) $R(\omega)$ in the THz range at 10 K. In the inset $R(\omega)$ is shown at 300 K up to 20000 cm^{-1}. (b) The real part of the optical conductivity showing a gap opening and a full recovery for $\omega > 6\Delta$, as expected for a BCS superconductor in the dirty limit. (c) The inverse square of the penetration depth, obtained from missing area in (b) (experimental points), is compared with the BCS dirty superconductor behavior, once normalized to zero temperature (grey line).

Below 6.3 K the zero-resistance regime is already established through a sharp transition, which confirms the good homogeneity of the film (see the dc resistance R_{dc} in the inset). However, by considering that the magnetization is a bulk quantity like the THz conductivity we assume here $T_c = 6$ K. In order to measure the superconducting gap, the sample was shined by the THz radiation produced when BESSY-II was set in the low-α operation mode [4]. In order to avoid any variation in the sample position and orientation, which may yield frequency-dependent systematic errors in the reflectivity, we cycled the temperature in the 2.6–15 K range without collecting reference spectra. Through this procedure $R_S(T)/R_N(10 \text{ K}) = I_S(T)/I_N(10 \text{ K})$, where I_S (I_N) is the intensity reflected by the sample in the superconducting (normal) state, and we obtained in the sub-THz range an error $\delta = I_S/I_N \sim 0.2\%$. The ratio $R_S(T)/R_N(10 \text{ K})$ is reported in Figure 1. The three curves at $T < T_c$ show a strong frequency dependence in the sub-THz region, with the predicted BCS peak at $\omega \sim 2\Delta(T)$. As a crosscheck, the data for $T > T_c$ do not show any peak and are equal to 1 within the
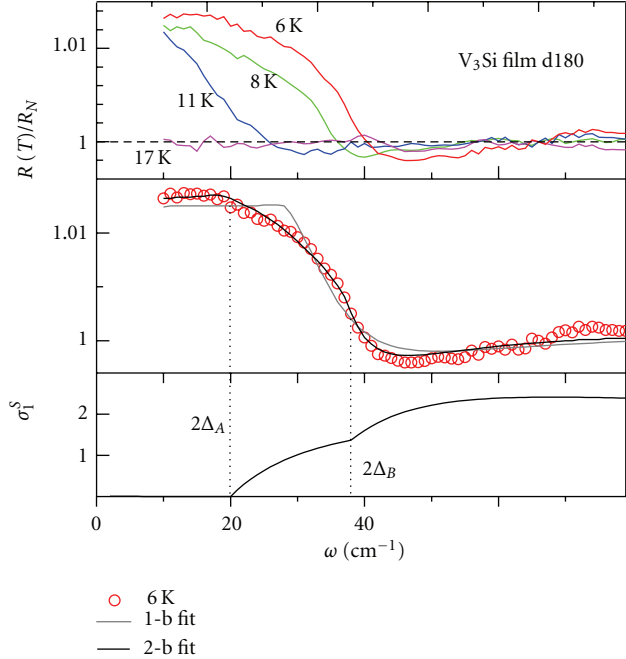
FIGURE 3: (a) $R(T)/R_N$(20K) ratio for the d180 film at selected temperatures in the THz region. (b) $R(6K)/R_N$(20K) ratio compared with the two-band (2-b) and single-band (1-b) best fit curves. (c) Real part of the optical conductivity in the superconducting state σ_1^S (in units $10^4\,\Omega^{-1}\,cm^{-1}$) of V_3Si from the 2-b model.

FIGURE 4: (a) $T_S(T)/T_N$(20K) spectra of the d33 film at selected temperatures in the THz region. (b) T_S (6K)/T_N(20K) spectrum compared with the two-band (2-b) and single-band (1-b) best fit curves. (c) Absorption coefficient in the superconducting state α_S (in units $10^4\,cm^{-1}$) of V_3Si from 2-b model.

noise. A first inspection to data at $T = 2.6$ K provides a peak value at $\sim 12\,cm^{-1}$, which gives $2\Delta(2.6\,K)/k_B T_c \sim 3$. Therefore we fit the data using a BCS approach [7]. The normal state reflectivity was described in terms of a Drude component whose parameters have been determined by the measurement at 10 K. In the superconducting state we used a Mattis-Bardeen modelization of R_S with a fixed $T_c = 6$ K and $\Delta(T)$ as a free fitting parameter.

The main output of the fit is the superconducting gap, which at 4.6, 3.4, and 2.6 K is found to be $2\Delta = 9.5$, 10.5, and $11.5\,cm^{-1}$, respectively. These values furnish an extrapolated value $2\Delta(0) = 12.5\,cm^{-1}$, or $2\Delta(0)/k_B T_c = 3.0 \pm 0.5$, in satisfactory agreement with the BCS prediction of 3.53 and ultraviolet photoemission spectroscopy [8] where the authors determined, at nearly 4 K, $2\Delta = 12.6\,cm^{-1}$.

Afterwards, we measured the absolute reflectivity R (both in the normal and in the superconducting state) up to $20000\,cm^{-1}$ taking as reference the film itself, coated with a gold or silver layer evaporated in situ. R_N at 300 K is represented in the inset of Figure 2(a) and shows a poor metallic behavior consistently with the relatively high dc resistivity value [7]. Through the standard Kramers-Kronig transformations we obtained the optical conductivity. The real part $\sigma_1(\omega)$, reported in Figure 2(b), decreases in the THz range for $T < T_c$, due to the opening of the superconducting gap. At 4.6 K, a residual quasiparticle contribution can still be distinguished at the lowest measured frequencies. At 2.6 K, a nearly zero absorption is attained below $\sim 10\,cm^{-1}$, a value comparable to 2Δ obtained from the reflectivity

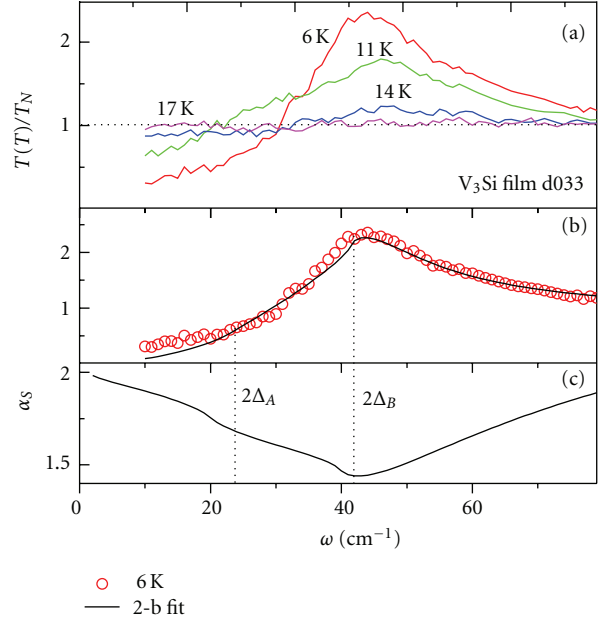ratio. One may notice that the optical conductivity of the superconducting phase $\sigma_1^S(\omega)$ and that of the normal phase $\sigma_1^N(\omega)$ in Figure 2(b) coincide for $\omega \sim 35\,cm^{-1} \sim 6\Delta$, indicating a BCS dirty limit behavior [1]. According to the Ferrell-Glover-Tinkham sum rule [1] the area A removed at $T < T_c$ below $\sigma_1(\omega, T)$, builds up the collective mode at $\omega = 0$. The spectral weight condensed into this peak may be used to extract the penetration depth $\lambda = 1/2\pi(8A)^{1/2}$ [1]. We thus estimate $\lambda \simeq 1\,\mu$m at 2.6 K. Finally, $1/\lambda^2$ is plotted in Figure 2(c) versus T/T_c, and compared with the BCS prediction for a dirty superconductor [1]. Once again, this model appears to well-describe the behavior here observed in B-doped diamond [7].

3. The Two-Gap Scenario in V_3Si

After the discovery of MgB_2 superconductor strong experimental and theoretical efforts have been devoted to multiband superconductivity [9], since several of the unique properties of this system are based on the presence of two bands with two distinct superconducting gaps [10]. In the case of the V_3Si system, which belongs to the A15 family contradictory results concerning the number of gaps opening below T_c have been published. Indeed, the study of the electrodynamics response in the microwave region gave evidence of two gaps [11] while muon spin rotation measurements are consistent with a single-gap scenario [12]. THz spectroscopy may help to solve this issue. On this regard we performed both reflectivity and transmittance
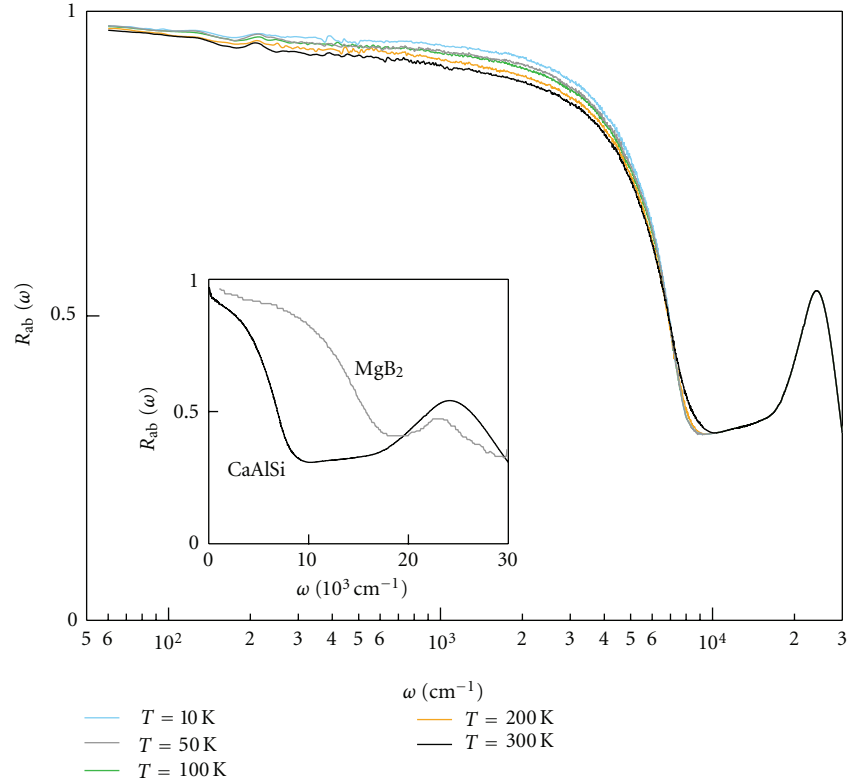
FIGURE 5: Reflectivity spectra of CaAlSi in the hexagonal plane at selected temperatures from the THz to the visible spectral region. In the inset a comparison between the reflectivity at 300 K of MgB_2 [2] and CaAlSi is shown.

measurements on high-quality V_3Si textured thin films. Details on the film growth by pulsed laser deposition and on their properties are reported elsewhere [13]. We studied two films deposited on $LaAlO_3$ (LAO) (001) 0.5 mm thick substrates, which exhibit preferential (210) orientation along the out-of-plane direction. The first film of thickness $d = 180$ nm (d180 film), characterized through reflectivity data, has good transport properties (resistivity at 300 K close to $200\,\mu\Omega$ cm, and at 20 K close to $25\,\mu\Omega$ cm) and $T_c = 16.1$ K. The second film with a thickness of 33 nm (d033 film) used for transmittance measurements, has a slightly lower T_c value ($T_c = 15.3$ K) probably due to the strain induced by the substrate on the film structure. Here, reflectivity and transmittance data in the THz range imposes a strong constraint in the fit parameters and provides a strong evidence of a two-gap scenario for the V_3Si system.

The $R_S(T)/R_N$ ratios (where $R_N = R_N$ (20 K)) at different $T < T_c$ for the d180 film are reported in Figure 3. These measurements were performed at the SISSI beamline [3] through the use of THz radiation produced by the ELETTRA machine [14], by cycling the temperature in the 6–20 K range, without collecting reference spectra. In this way one avoids any variation in the sample position and orientation, which may yield frequency-dependent systematic errors both in reflectivity $R(\omega)$ and transmittance $T(\omega)$. We first notice that the $R_S(T)/R_N$ ratio (Figure 3(a)) increases on decreasing temperature until it reaches a maximum and becomes nearly

constant below 20 cm^{-1}. This indicates a superconducting gap Δ_A closes to 10 cm^{-1}. Indeed, for $\omega \to 0$ the reflectance R_N of a metallic system tends to 1 in the case of a bulk system, and to a slightly lower value for a thin film. Therefore, as discussed in the introduction, when R_S approaches 1 at $\omega = 2\Delta$, R_S/R_N exhibits a maximum around 2Δ in the case of a bulk sample, while it remains nearly constant below 2Δ in the case of a thin film. Instead in $T_S(T)/T_N$ (20 K) data (see Figure 4(a)), a broad maximum develops on decreasing T until, at 6 K, $T_S(T)/T_N$ exhibits a well-defined peak around 40 cm^{-1}. Therefore, in superconducting films, the combination of transmission and reflection spectroscopy is essential to extract from optical data the superconducting parameters.

This peak is consistent with the presence of a superconducting gap Δ_B at about 20 cm^{-1}. We point out that the high-flux synchrotron source allows us a high accuracy in the detection of small effects in the $R_S(T)/R_N$ spectra and overcomes the problem of the very low intensity transmitted by the film + substrate system in the case of transmission measurements on a conducting film. We also note that $T_S(T)/T_N$ is affected by the superconducting transition much more than $R_S(T)/R_N$ as the transmitted intensity is mainly controlled by the strong absorptive processes in the film, which significantly changes below T_c.

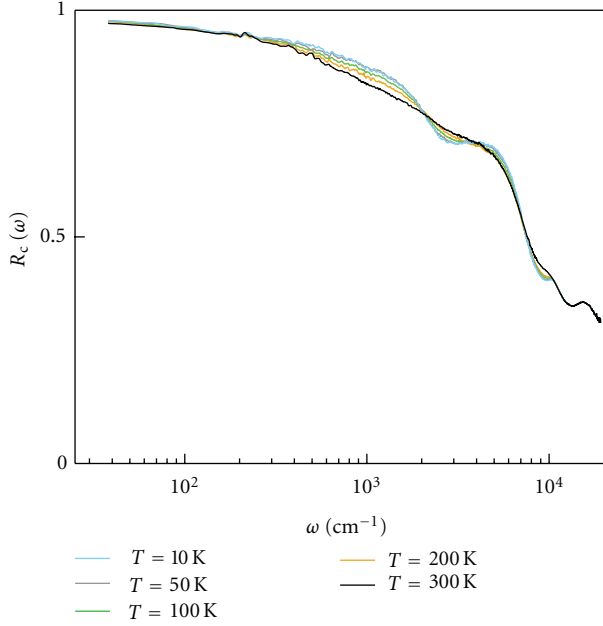In order to perform a detailed analysis of the transmittance and reflectivity spectra, the complex refraction index of

FIGURE 6: Reflectivity spectra of CaAlSi along the c-axis at selected temperatures from 50 to 30000 cm^{-1}.

V_3Si has been described in the normal state through the sum of two Drude terms (related to the main conduction bands crossing E_F), with parameters ω_{pA} (3.7 ± 0.1 eV), $\Gamma_A(T)$ (800 ± 40 cm^{-1}), and ω_{pB} (1.00 ± 0.05 eV), $\Gamma_B(T)$ (45 ± 4 cm^{-1}). The superconducting spectra have been described through a Mattis-Bardeen refraction index depending on the gap $\Delta(T)$ [1]. Finally the transmittance and reflectance spectra of the film + substrate system in both states can then be evacuated by means of an exact procedure [15] which requires, besides thickness, the values of for both film and substrate. For LAO, values in the THz region were obtained from previous measurements of transmittance and reflectance [14].

By using the previous procedure a single gap description cannot take into account either the shape or the T dependence of $R_S(T)/R_N$ ratio (blue line in Figure 3(b)). On the other hand $R_S(T)/R_N$ and $T_S(T)/T_N$ ratios agree well with a two-gap scenario (black lines in Figures 3(b) and 4(b)), that is also consistent with two main electronic bands crossing the Fermi energy [16].

From the reflectivity ratio at $T = 0$ and from the two-gap fit, one obtains $\Delta_A(0) = 10 \pm 1$ cm^{-1}, and $\Delta_B(0) = 19 \pm 2$ cm^{-1}, while from the transmittance measurements, which are less sensitive to the low energy gap (see [16]), $\Delta_A(0)$ ranges from 11 to 16 cm^{-1} and $\Delta_B = 21.0 \pm 0.5$ cm^{-1}. The comparison of $2\Delta_{A(B)}$ with the corresponding scattering rate $\Gamma_A = 800$ cm^{-1} ($\Gamma_B = 45$ cm^{-1}) shows that V_3Si is in a dirty limit regime. Moreover, the gap values correspond to BCS ratios of $2\Delta_B(0)/k_BT_c = 3.8 \pm 0.3$ and $2\Delta_A(0)/k_BT_c = 1.8 \pm 0.2$, respectively. While the former ratio agrees with a standard BCS weak coupling, the latter, which is instead in agreement with tunneling data [17], indicates an anomalous superconducting weak coupling that

are related to the specific electronic density of states in which this small gap opens [16].

4. The Anisotropic Gaps of CaAlSi.

CaAlSi is a recently discovered superconductor characterized by a T_c of 7.7 K and hole transport [18]. It has attracted wide interest for its properties including the hexagonal crystal structure similar to that of MgB_2, where however the carriers are electrons. Like MgB_2, CaAlSi has two Fermi-surface sheets. However, it is not clear if one should expect one gap or two gaps like in MgB_2. CaAlSi has an s-wave anisotropic symmetry [19] probably related to the hexagonal crystal structure. Angle resolved photoemission (ARPES) [20], within the energy resolution, distinguished in CaAlSi a single isotropic gap of about 1.2 meV = 4.2 k_BT_c. Muon spin relaxation (μR) data [2] indicated a highly anisotropic gap, or possibly two distinct gaps like in MgB_2. Finally penetration depth measurements [19] support weakly anisotropic s-wave gap, but not two distinct gaps. THz spectroscopy, which allows one to measure the gap directly and with a resolution in energy higher than in ARPES, may help to solve this issue, provided that one attains a suitable signal-to-noise ratio. Here we measured a CaAlSi single crystal with a size of $2 \times 4.5 \times 3$ mm^3 [18]. Its magnetic moment $M(T)$ (see the upper inset in Figure 7) shows the superconducting transition with an onset at 6.7 K.

In Figure 5 we represent the reflectivity in the hexagonal plane measured at different T in the normal phase from 50 to 30000 cm^{-1}. At variance with B-doped diamond (see Figure 2(a)) $R_{ab}(\omega)$ looks like that of a good metal. Below the plasma edge around 10000 cm^{-1}, and at any $T > T_c$, the reflectivity can be well described by a conventional Drude model with a bare plasma frequency $\omega_p(ab) = 20000$ cm^{-1} independent of T and a scattering rate $\Gamma_{ab}(T) = 480$ cm^{-1} and 850 cm^{-1} at 10 and 300 K, respectively. The corresponding $\omega_p(ab)$ for MgB_2 (see the inset of the same figure) is instead nearly 45000 cm^{-1} [21].

In Figure 6 we show instead the c-axis reflectivity at various T in the normal state. At variance with the ab reflectivity the low-energy properties along the c-axis cannot be described in terms of a single Drude term. Indeed we observed interband transitions at 4000, 9000, and 12000 cm^{-1} superimposed to a Drude component with a bare $\omega_p(c) = 9000$ cm^{-1} and a $\Gamma_c(T)$ of 180 cm^{-1} at 10 K, 235 cm^{-1} at 300 K [22]. By comparing Figures 5 and 6 we can note that CaAlSi presents a quite strong normal-state anisotropic behavior which will be also observed in the superconducting state (see below).

The ratio $R_{ab}(T)/R_{ab}(10 K)$ is reported in Figure 7 for the radiation polarized in the hexagonal plane at different T, both below and above T_c. The curves at $T < T_c$ exhibit the expected peak at $2\Delta_{ab}(T)$, while for $T > T_c$ (12 K), the above ratio is equal to 1 at any ω within the noise. In order to extract the gap the reflectivity ratios have been fitted by using the Drude parameters $\omega_p(ab)$ and $\Gamma_{ab}(T)$ determined from the normal state reflectivity and using the Mattis-Bardeen model for the superconducting state with a
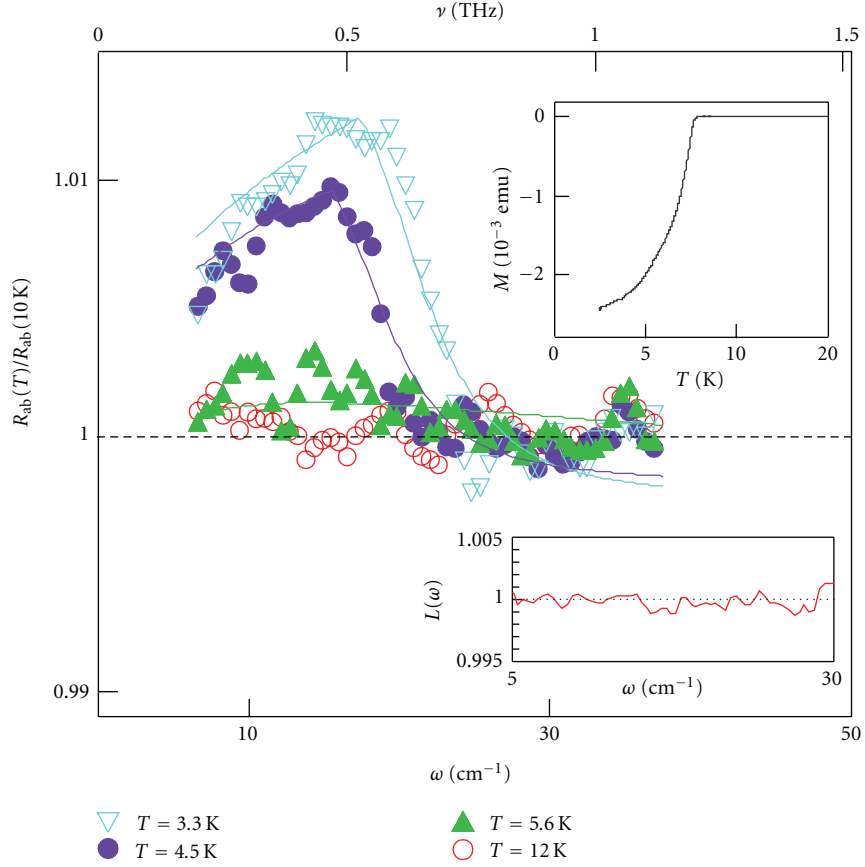
FIGURE 7: Ratio between the sub-THz reflectivity of the ab planes below T_c and in the normal phase at 10 K. The lines are fits based on a Mattis-Bardeen reflectivity below T_c and on a Drude model at 10 K (see text). The upper inset shows the magnetic moment measured by cooling the sample in a field of 10 Oe, showing the superconducting transition at $T_c = 6.7$ K. The lower inset shows a check on data reproducibility, performed by dividing two subsequent spectra of 256 scans.

fixed $T_c = 6.7$ K and $\Delta_{ab}(T)$ as free parameter. The curves $R_{ab}(T)/R_{ab}(10\ K)$ calculated in this way are also reported in Figure 7 (thin lines). The fit is good at the three temperatures below T_c and provides $2\Delta_{ab} = 15$ and $17.5\ cm^{-1}$ at 4.5 and 3.3 K, respectively. This leads to an extrapolated value $2\Delta_{ab}(0) = 19.0 \pm 1.5\ cm^{-1}$ or $2\Delta_{ab}(0)/k_B T_c = 4.1 \pm 0.4$, a value which is in substantial agreement with ARPES data [18]. The actual $2\Delta_{ab}(0)/k_B T_c$ ratio suggests that CaAlSi is a BCS superconductor with moderately strong electron-phonon coupling. On the basis of our fits, which take into account both the measured data in the normal and in the superconducting state, a single gap well-describes the superconducting transition in the hexagonal planes.

Let us now consider the optical response of CaAlSi along the c-axis. Figure 8 shows the ratio $R_c(T)/R_c(10\ K)$, as measured with the radiation polarized along the c direction. A peak appears below T_c, but its different shape with respect to those in Figure 7. Such a shape suggests that either only a fraction of the carriers contributes to the optical conductivity of the superconducting phase or there are, at least, two distinct gaps. The former case is observed, for example, in high-T_c cuprates, where the order parameter has nodes in the k space due to its d-wave symmetry, but this should be excluded in CaAlSi where the main conducting electronic bands around E_F have a highly symmetric character. The latter case has been observed in MgB_2, where a two-gap model well-accounts for the reflectivity data below T_c. In CaAlSi, the two gaps should come out from different regions of the Fermi surface, which are topologically disconnected along the k_z direction [23]. A two-gap model well-fit the $R_c(T < T_c)/R_c(10\ K)$ data of Figure 8 (solid lines) and the results for the larger gap are $2\Delta_{c,1} = 22\ cm^{-1}$ at 4.5 K, $26\ cm^{-1}$ at 3.3 K, and $28\ cm^{-1}$ extrapolated to 0 K; instead the fit provides for the smaller gap: $2\Delta_{c,2} = 2,\ 6,$ and $8\ cm^{-1}$ at 4.5, 3.3 and 0 K, respectively. The very low value for the $\Delta_{c,2}$ may be related to a specific electronic density of states in which this small gap opens.

Finally, the comparison between the scattering rate at 10 K $\Gamma_{ab}(T) = 480\ cm^{-1}(\Gamma_c(T) = 180\ cm^{-1})$ and $2\Delta_{ab}(0) = 19.0\ cm^{-1}\ (2\Delta_c(0) = 28\ cm^{-1})$ shows that, both in the ab plane, and along the c axis, CaAlSi is also in the dirty limit regime.
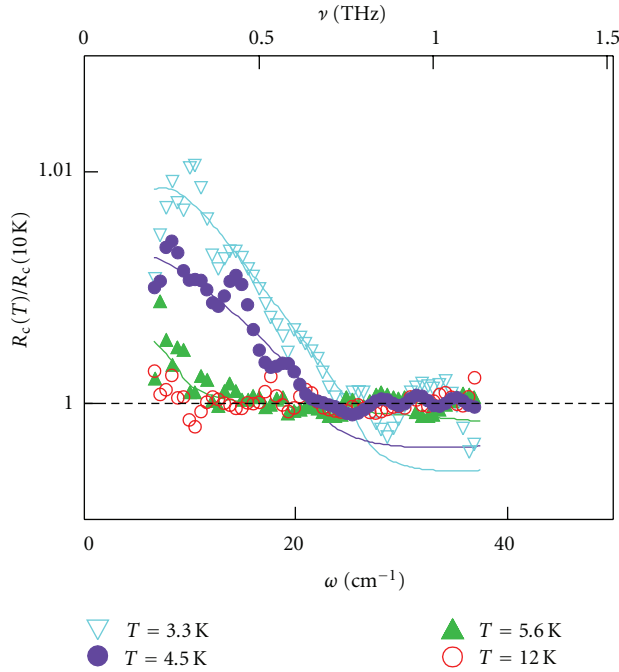
FIGURE 8: Ratio between the sub-THz reflectivity along the c-axis below T_c and in the normal phase at 10 K. The lines are fits based on a BCS reflectivity below T_c and on a Drude-Lorentz model at 10 K (see text).

In this experimental review we have shown some applications of frequency-domain THz spectroscopy in superconductivity. THz radiation extracted from the III generation synchrotron machines ELETTRA and BESSY-II coupled with Michelson interferometry, provides the possibility to investigate the bulk properties of novel superconductors in their normal and superconducting state. In particular we have determined the superconducting gap for the B-doped diamond, V$_3$Si (A15 type), and CaAlSi (MgB$_2$ type) superconductors. This technique provides a signal-to-noise ratio of the order of 10^3, which is needed to appreciate the weak increase (decrease) in the reflectivity (transmittance) across the critical temperature T_c. We have shown that B-doped diamond is an isotropic superconductor characterized by a ratio $2\Delta(0)/k_B T_c = 3.0 \pm 0.5$, in satisfactory agreement with the theoretical BCS prediction of 3.53. In CaAlSi, which has a crystal structure similar to that of MgB$_2$, we have determined the superconducting gap both in the hexagonal ab planes and along the orthogonal c-axis. Here $2\Delta_{ab}(0) < 2\Delta_c(0)$ showing that CaAlSi is a BCS anisotropic s-wave superconductor. We have also addressed the debated problem of multiband, multigap nature of A15 type V$_3$Si superconductor by means of reflectance and transmittance measurements in the THz region. Our experimental results indicate that in the two main electronic bands crossing E_F two gaps of different magnitude open below T_c. This result is of current interest, especially after the discovery of the Fe-based superconductors, as it addresses multigap superconductivity in a system where complications coming from magnetism and nodal symmetries do not arise.

However, frequency domain spectroscopy does not exhaust all potentialities of THz radiation. Indeed the recent development of strong, femtosecond, THz pulses [24, 25] may open a new route in THz spectroscopy. These pulses should be used in time resolved THz-pump THz-probe investigations to probe the intrinsic dynamics of Cooper pairs and their relaxation towards a steady state. A new fascinating scenario could be also open through the control and the manipulation of the superconducting transition by using the intense electric and magnetic fields associated with the femto-second THz pulses [26].

Acknowledgments

References

[1] M. Dressel and G. Gruner, *Electrodynamics of Solids. Optical Properties of Electrons in Matter*, Cambridge University Press, 2002.

[2] S. Tsuda, T. Yokoya, S. Shin, M. Imai, and I. Hase, "Identical superconducting gap on different Fermi surfaces of Ca(Al Si) with the AlB structure," *Physical Review B*, vol. 69, no. 10, Article ID 100506, pp. 1–4, 2004.

[3] S. Lupi, A. Nucara, A. Perucchi et al., "Performance of SISSI, the infrared beamline of the ELETTRA storage ring," *Journal of the Optical Society of America B*, vol. 24, no. 4, pp. 959–964, 2007.

[4] M. Abo-Bakr, J. Feikes, K. Holldack, P. Kuske, W. B. Peatman, and U. Schade, "Brilliant, coherent far-infrared (THz) synchrotron radiation," *Physical Review Letters*, vol. 90, no. 9, Article ID 094801, pp. 1–4, 2003.

[5] Y. Takano, M. Nagao, I. Sakaguchi et al., "Superconductivity in diamond thin films well above liquid helium temperature," *Applied Physics Letters*, vol. 85, no. 14, pp. 2851–2853, 2004.

[6] T. Yokoya, T. Nakamura, T. Matsushita et al., "Origin of the metallic properties of heavily boron-doped superconducting diamond," *Nature*, vol. 438, no. 7068, pp. 647–650, 2005.

[7] M. Ortolani, S. Lupi, L. Baldassarre et al., "Low-energy electrodynamics of superconducting diamond," *Physical Review Letters*, vol. 97, no. 9, Article ID 097002, 2006.

[8] K. Ishizaka, R. Eguchi, S. Tsuda et al., "Observation of a superconducting gap in boron-doped diamond by laser-excited photoemission spectroscopy," *Physical Review Letters*, vol. 98, no. 4, Article ID 047003, 2007.

[9] F. Bouquet, Y. Wang, I. Sheikin et al., "Specific heat of single crystal MgB$_2$: a two-band superconductor with two different anisotropies," *Physica C*, vol. 89, no. 25, Article ID 257001, p. 4, 2002.

[10] J. Kortus, I. I. Mazin, K. D. Belashchenko, V. P. Antropov, and L. L. Boyer, "Superconductivity of metallic Boron in MgB2," *Physical Review Letters*, vol. 86, no. 20, pp. 4656–4659, 2001.

[11] Y. A. Nefyodov, A. M. Shuvaev, and M. R. Trunin, "Microwave response of vSi single crystals: evidence for two-gap superconductivity," *Europhysics Letters*, vol. 72, no. 4, pp. 638–644, 2005.

[12] J. E. Sonier, F. D. Callaghan, R. I. Miller et al., "Shrinking magnetic vortices in VSi due to delocalized quasiparticle core states: confirmation of the microscopic theory for interacting vortices," *Physical Review Letters*, vol. 93, no. 1, Article ID 017002, p. 1, 2004.

[13] C. Ferdeghini, E. Bellingeri, C. Fanciulli et al., "Superconducting properties of VSi thin films grown by pulsed laser ablation," *IEEE Transactions on Applied Superconductivity*, vol. 19, no. 3, pp. 2682–2685, 2009.

[14] P. Dore, G. P. Gallerano, A. Doria, E. Giovenale, R. Trippetti, and V. Boffa, " Study of the far-infrared and mm-wave conductivity of YBCO in the normal state," *Il Nuovo Cimento D*, vol. 16, no. 10-11, pp. 1803–1807, 1994.

[15] S. Cunsolo, P. Dore, and C. P. Varsamis, "Refractive index of crystals from transmission and reflection measurements: MgO in the far-infrared region," *Applied Optics*, vol. 31, no. 22, pp. 4554–4558, 1992.

[16] A. Perucchi, D. Nicoletti, M. Ortolani et al., "Multiband conductivity and a multigap superconducting phase in V_3Si films from optical measurements at terahertz frequencies," *Physical Review B*, vol. 81, no. 9, Article ID 092509, 2010.

[17] N. Hauptmann, M. Becker, J. Kröger, and R. Berndt, "Surface reconstruction and energy gap of superconducting V3 Si (001)," *Physical Review B*, vol. 79, no. 14, Article ID 144522, 2009.

[18] A. K. Ghosh, M. Tokunaga, and T. Tamegai, "Angular dependence of the upper critical field in CaAlSi single crystal: deviation from the Ginzburg-Landau anisotropic mass model," *Physical Review B*, vol. 68, no. 5, pp. 545071–545075, 2003.

[19] R. Prozorov, T. A. Olheiser, R. W. Giannetta, K. Uozato, and T. Tamegai, "Anisotropic s-wave superconductivity in CaAlSi single crystals from penetration depth measurements," *Physical Review B*, vol. 73, no. 18, Article ID 184523, 2006.

[20] S. Kuroiwa, H. Takagiwa, M. Yamazawa et al., "Unconventional behavior of field-induced quasiparticle excitation in Ca(AlSi)," *Journal of the Physical Society of Japan*, vol. 73, no. 10, pp. 2631–2634, 2004.

[21] C. Mirri, "Exotic superconductors: an infrared spectroscopy study," Ph.D. thesis, University of Rome La Sapienza, 2010.

[22] S. Lupi, L. Baldassarre, M. Ortolani et al., "Subterahertz electrodynamics of the graphenelike superconductor CaAlSi," *Physical Review B*, vol. 77, no. 5, Article ID 054510, 2008.

[23] M. Giantomassi, L. Boeri, and G. B. Bachelet, "Electrons and phonons in the ternary alloy CaAl2-xSix as a function of composition," *Physical Review B*, vol. 72, no. 22, Article ID 224512, pp. 1–9, 2005.

[24] M. Ferrario, D. Alesini, A. Bacci et al., "Laser comb with velocitybunching: preliminary results at SPARC," *Nuclear Instrument and Methods A*. In press.

[25] "DOE-NSF-NIH Workshop on Opportunities in THz Science," 2004, http://www.er.doe.gov/bes/reports/files/THz_rpt.pdf.

[26] Y. Shen, T. Watanabe, D. A. Arena et al., "Nonlinear cross-phase modulation with intense single-cycle terahertz pulses," *Physical Review Letters*, vol. 99, no. 4, Article ID 043901, 2007.

Journal of
Gravity

Journal of
Photonics

The Scientific
World Journal

Journal of
Soft Matter

Advances in
Condensed Matter Physics

Journal of
Fluids

Journal of
Aerodynamics

International Journal of
Statistical Mechanics

Hindawi

Submit your manuscripts at
http://www.hindawi.com

International Journal of
Optics

Journal of
Computational
Methods in Physics

Advances in
High Energy Physics

Journal of
Thermodynamics

Physics
Research International

Advances in
Astronomy

Journal of
Solid State Physics

Journal of
Astrophysics

International Journal of
Superconductivity

Journal of
Biophysics

Journal of
Atomic and
Molecular Physics